Journal of Vibration Engineering & Technologies (2022) 10:1253–1264
https://doi.org/10.1007/s42417-022-00441-y

ORIGINAL PAPER

Content-Dependent Nonlinear Vibration of Composite Plates Reinforced with Carbon Nanotubes

W. Zhang[1] · L. J. He[1] · J. F. Wang[1]

Received: 25 December 2021 / Revised: 31 January 2022 / Accepted: 5 February 2022 / Published online: 23 February 2022

Abstract

Purpose In this paper, the nonlinear vibration behavior of functionally graded carbon nanotube reinforced composite (FG-CNTRC) plates is investigated by meshless method.

Methods The efficiency parameters, which clearly affect the mechanical properties of the composite materials, are characterized by polynomial expressions for different CNT contents, and applied as the inputs in the vibration analysis of plate structure. Four distributions of CNTs along the thickness of composite plate are considered, namely, the uniform distribution (UD), FG-O, FG-X and FG-V. Based on the classical plate theory and von Karman strain-displacement relation, the governing equations of motion are derived by the virtual displacement principle. Based on the reproducing kernel particle method (RKPM), the discrete governing equations for the vibration of the FG-CNTRC plates are derived. The linearized updated mode (LUM) method is adopted to solve the iteration process of governing equations.

Results Numerical results are employed to investigate the effects of boundary condition, aspect ratio, volume fraction and arrangement of CNT on the nonlinear vibration characteristics of composite plates.

Keywords Nonlinear vibration · Carbon nanotube · Functionally graded material · Efficiency parameter · Reproducing kernel particle method

Introduction

Composite with nano-reinforcement is widely used in engineering applications such as aerospace, marine, automotive owing to the high strength and stiffness. As an ideal reinforcement for composite structures, carbon nanotubes (CNTs) demonstrate the excellent mechanical, electrical and thermal properties [1–4]. Scientists and engineers have raised huge interest to promote the development of CNT-based composites in fundamental research and application [5–7]. Functionally graded materials (FGMs) were proposed by Bever and Duwez [8], in which the volume fraction of reinforcement was changed by layers along the thickness direction of composite structures, and the resulting material properties were changed smoothly and effectively [9, 10]. By introducing the concept of the FGMs into the CNT-based composites, Shen [11] proposed functionally graded carbon nanotube reinforced composite (FG-CNTRC), and the further study about nonlinear bending behavior and large amplitude vibration demonstrated the effect of CNT distribution on the frequency and deflection of FG-CNTRC plates [12].

Composite materials can be custom tailored to meet the specific requirements of particular structures. In the process of design, it is necessary to analyze and predict the mechanical property with scale effect taken into account [13]. Wang et al. [14] investigated the thermal vibration and buckling of FG-CNTRC quadrilateral plates, and presented the effects of CNT volume fraction and distribution on the natural frequency and critical buckling load. Chiker et al. [15] studied the influence of CNT distribution on the vibrational behavior of nanocomposite plates, and the results indicated that compared with the FG-based plates with uniform CNT distribution, the natural frequencies of FG-X and FG-O CNTRC plates were increased and decreased, respectively. Tang and Dai [16] established the mechanical model of CNTRC plates with different CNT distributions to discuss the effects of geometrical size, volume fraction and damping coefficient on the nonlinear vibration behaviors.

✉ J. F. Wang
jf.wang@bjut.edu.cn

[1] Beijing Key Laboratory of Nonlinear Vibrations and Strength of Mechanical Structures, Faculty of Materials and Manufacturing, Beijing University of Technology, Beijing 100124, China

The effective material parameters of composites are of great significance to study the mechanical behavior of structures, which are generally evaluated by Halpin-Tsai micromechanics model or the rule of mixtures. Nevertheless, the difference between the homogenization approach and molecular dynamics (MD) simulation could not be neglected due to the nano-scale effect. Shen and Zhang [17] incorporated the CNT efficiency parameters under a specific CNT volume fraction by matching Young's moduli of CNTRC via the rule of mixtures with the MD results obtained by Han and Elliott [18]. It is noticed that the value of CNT efficiency parameter may be variable according to different CNT volume fractions. Wang et al. [19] derived the polynomial expression of efficiency parameters for composites with different CNT volume fractions, and extended to the vibration analysis of composite plates. Based on that, the adjacent macro- and micro-scale of material properties are connected, and the quantitative transfer across scales are achieved.

A considerable number of experimental and numerical methods have been developed rapidly and applied successfully to investigate the mechanical behaviors of CNTRC plates. Mehar et al. [20, 21] carried out three-point bending test and impact hammer test to analyze the bending and vibration behaviors of CNTRC plate, respectively. Fantuzzi et al. [22] performed the free vibration of arbitrarily shaped FG-CNTRC plates by generalized differential quadrature (GDQ) method. Gupta and Talha [23] discussed the effects of geometrical parameter and boundary condition on the vibration response of FG plates with finite element method (FEM). Mesh distortion problem is usually encountered when dealing with large deformations, and lead to reduced accuracy and expensive computational effort because of the additional error during remeshing procedure [24, 25]. Meshless method was proposed to eliminate the above-mentioned problem, which has been widely used in the vibration analysis of composite plates [26–30]. Esfahani et al. [31] incorporated the reproducing kernel particle method (RKPM) into finite strip method (FSM) to study the free vibration of rectangular FG plates. Shukla et al. [32] used the radial basis function (RBF) to analyze the free vibration of angular laminates. Wang et al. [33] adopted the solution of the RKPM to study the nonlinear vibration of composite rectangular plates. Kazemi et al. [34] carried out the nonlinear dynamic analysis of FG-CNTRC cylinders by the meshless local Petrov Galerkin (MLPG) method.

The present work is focused on the nonlinear free vibration of FG-CNTRC plates by meshless method. The effective material parameters including Young's and shear moduli are derived by the extended rule of mixtures. Based on the classical plate theory and nonlinear strain-displacement relation, the governing equations of motion are derived by the virtual displacement principle. The numerical results demonstrate the effects of boundary condition, aspect ratio, volume fraction and the distribution of CNTs on the nonlinear vibration characteristics of FG-CNTRC plates.

Formulations for FG-CNTRC Plates

According to the classical plate theory, the displacements of FG-CNTRC plates along the x, y and z directions are defined as

$$u(x,y,z,t) = u_0(x,y,t) - zw_{0,x}(x,y,t), \tag{1a}$$

$$v(x,y,z,t) = v_0(x,y,t) - zw_{0,y}(x,y,t), \tag{1b}$$

$$w(x,y,z,t) = w_0(x,y,t), \tag{1c}$$

where u, v, and w are the displacements of an arbitrary point along x, y, and z directions, respectively, and u_0, v_0, and w_0 are the mid-plane displacements in the FG-CNTRC plate. The strain-displacement relation is defined as

$$\varepsilon_x^0 = u_{,x} + \frac{1}{2}\left(w_{,x}\right)^2, \tag{2a}$$

$$\varepsilon_y^0 = v_{,y} + \frac{1}{2}\left(w_{,y}\right)^2, \tag{2b}$$

$$\varepsilon_{xy}^0 = u_{,y} + v_{,x} + w_{,x}w_{,y}. \tag{2c}$$

$$\kappa_x = -w_{,xx}, \tag{3a}$$

$$\kappa_y = -w_{,yy}, \tag{3b}$$

$$\kappa_z = -2w_{,xy}. \tag{3c}$$

Therefore, the in-plane and shear strains are expressed as

$$\boldsymbol{\varepsilon} = \begin{bmatrix} \varepsilon_x \\ \varepsilon_y \\ \varepsilon_{xy} \end{bmatrix} = \begin{bmatrix} \varepsilon_x^0 \\ \varepsilon_y^0 \\ \varepsilon_{xy}^0 \end{bmatrix} + z\begin{bmatrix} \kappa_x \\ \kappa_y \\ \kappa_z \end{bmatrix} = \boldsymbol{\varepsilon}^0 + z\boldsymbol{\kappa}, \tag{4}$$

where $\boldsymbol{\varepsilon}^0$ is the mid-plane strain, and $\boldsymbol{\kappa}$ is the curvature. The constitutive relation of CNTRC plates is expressed as

$$\boldsymbol{\sigma} = \begin{bmatrix} \sigma_x \\ \sigma_y \\ \sigma_{xy} \end{bmatrix} = \begin{bmatrix} Q_{11} & Q_{12} & 0 \\ Q_{12} & Q_{22} & 0 \\ 0 & 0 & Q_{66} \end{bmatrix} \begin{bmatrix} \varepsilon_x \\ \varepsilon_y \\ \varepsilon_{xy} \end{bmatrix} = \boldsymbol{Q}\boldsymbol{\varepsilon}, \tag{5}$$

where Q_{ij} are given as

$$Q_{11} = \frac{E_{11}}{1-\nu_{12}\nu_{21}}, Q_{22} = \frac{E_{22}}{1-\nu_{12}\nu_{21}},$$
$$Q_{12} = \frac{\nu_{21}E_{22}}{1-\nu_{12}\nu_{21}} = \frac{\nu_{21}E_{11}}{1-\nu_{12}\nu_{21}}, Q_{66} = G_{12}, \tag{6}$$

and E_{11}, E_{22}, and G_{12} are the effective longitudinal, transverse and shear moduli, respectively. The moduli are determined by

$$E_{11} = \eta_1 V_{\mathrm{CNT}} E_{\mathrm{CNT}}^{11} + V_{\mathrm{m}} E_{\mathrm{m}}, \tag{7a}$$

$$\frac{\eta_2}{E_{22}} = \frac{V_{\mathrm{CNT}}}{E_{\mathrm{CNT}}^{22}} + \frac{V_{\mathrm{m}}}{E_{\mathrm{m}}}, \tag{7b}$$

$$\frac{\eta_3}{G_{12}} = \frac{V_{\mathrm{CNT}}}{G_{\mathrm{CNT}}^{12}} + \frac{V_{\mathrm{m}}}{G_{\mathrm{m}}}, \tag{7c}$$

where E_{CNT}^{11}, E_{CNT}^{22} and G_{CNT}^{12} indicate Young's moduli of CNT along the longitudinal and transverse directions and shear modulus, η_1, η_2 and η_3 are the corresponding efficiency parameters, E_{m} and G_{m} represent Young's and shear moduli of the matrix.

The FG-CNTRC plates with four distributions of CNT are shown in Fig. 1, and the dimensions are length a, width b and thickness h. The effective volume fractions of FG-CNTRC plates are expressed as

$$V_{\mathrm{CNT}}^{*} = V_{\mathrm{CNT}}, \mathrm{UD}, \tag{8a}$$

$$V_{\mathrm{CNT}}^{*}(z) = \left(1 + \frac{2z}{h}\right) V_{\mathrm{CNT}}, \mathrm{FG\ -\ V}, \tag{8b}$$

$$V_{\mathrm{CNT}}^{*}(z) = 2\left(1 - \frac{2|z|}{h}\right) V_{\mathrm{CNT}}, \mathrm{FG\ -\ O}, \tag{8c}$$

$$V_{\mathrm{CNT}}^{*}(z) = \left(\frac{4|z|}{h}\right) V_{\mathrm{CNT}}, \mathrm{FG\ -\ X}, \tag{8d}$$

where V_{CNT}^{*} is the corresponding CNT volume fraction of each layer, V_{CNT} is the total CNT volume fraction of composite plate. The volume fractions of composite components are denoted as

$$V_{\mathrm{CNT}} + V_{\mathrm{m}} = 1, \tag{9}$$

where V_{m} is the volume fraction of matrix. The material parameters including Poisson's ratio and density are determined by volume fractions as

$$\nu_{12} = V_{\mathrm{CNT}} \nu_{\mathrm{CNT}}^{12} + V_{\mathrm{m}} \nu_{\mathrm{m}}, \tag{10}$$

$$\rho = V_{\mathrm{CNT}} \rho_{\mathrm{CNT}} + V_{\mathrm{m}} \rho_{\mathrm{m}}, \tag{11}$$

where ρ_{m} and ρ_{CNT} are the densities of matrix and CNT, respectively. The in-plane and transverse shear force resultants are defined as

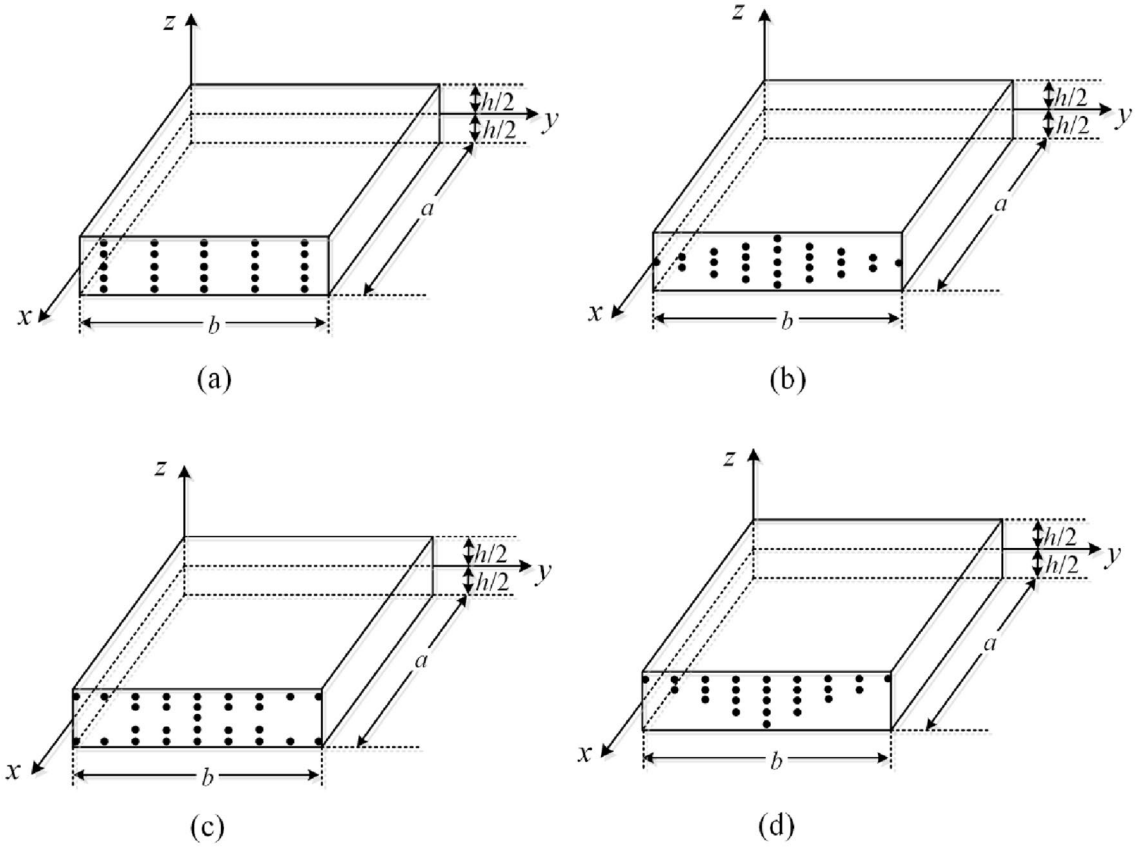

Fig. 1 Configurations of carbon nanotube reinforced composite plates including **a** UD; **b** FG-O; **c** FG-X; **d** FG-V

$$(\boldsymbol{N},\boldsymbol{M}) = \int_{z_{k-1}}^{z_k} (1,z)\boldsymbol{\sigma}\mathrm{d}z. \tag{12}$$

By substituting Eq. (5) into Eq. (12), the stress and moment resultants are obtained as follows

$$\boldsymbol{N} = \boldsymbol{A}\boldsymbol{\varepsilon}^0 + \boldsymbol{B}\boldsymbol{\kappa}, \tag{13}$$

$$\boldsymbol{M} = \boldsymbol{B}\boldsymbol{\varepsilon}^0 + \boldsymbol{D}\boldsymbol{\kappa}. \tag{14}$$

where $\boldsymbol{A}$, $\boldsymbol{B}$, and $\boldsymbol{D}$ are the in-plane, coupled bending-stretching, and bending stiffness matrices, respectively, which are given by

$$(\boldsymbol{A},\boldsymbol{B},\boldsymbol{D}) = \int_{z_{k-1}}^{z_k} \left(1,z,z^2\right)\boldsymbol{Q}\mathrm{d}z. \tag{15}$$

According to the principle of virtual work

$$\delta W_{\mathrm{in}} + \delta W_{\mathrm{ex}} = 0, \tag{16}$$

$$\delta W_{\mathrm{ex}} = \int_{\Omega} \rho h\left(\delta u_0\ddot{u} + \delta v_0\ddot{v} + \delta w_0\ddot{w}\right)\mathrm{d}\Omega, \tag{17}$$

$$\delta W_{\mathrm{in}} = \int_{\Omega} \left(\delta \boldsymbol{N}^{\mathrm{T}}\boldsymbol{\varepsilon}^0 + \delta \boldsymbol{M}^{\mathrm{T}}\boldsymbol{\kappa}\right)\mathrm{d}\Omega, \tag{18}$$

where δW_{in} and δW_{ex} are the work done by the inertial force and the elastic restoring force, respectively.

After that, the motion equation of composite plate is derived by setting the sum of virtual works as zero. Based on the von Karman strain–displacement relation and the principle of virtual work, we get

$$\int_{\Omega} \rho h\left(\delta u_0\ddot{u} + \delta v_0\ddot{v} + \delta w_0\ddot{w}\right)\mathrm{d}\Omega + \int_{\Omega} \left(\delta \boldsymbol{N}^{\mathrm{T}}\boldsymbol{\varepsilon}^0 + \delta \boldsymbol{M}^{\mathrm{T}}\boldsymbol{\kappa}\right)\mathrm{d}\Omega = 0. \tag{19}$$

Solution Procedure

By introducing a correction function in the reproduction formula of the smooth particle hydrodynamics, RKPM is proposed to modify the kernel function and enhance the accuracy [35]. The whole domain Ω is assumed to be discretized by the particles (x_1, x_2, …, x_{N}), and the approximation of displacement is expressed as

$$\begin{bmatrix} u_0 \\ v_0 \\ w_0 \end{bmatrix} = \sum_{\mathrm{I}=1}^{\mathrm{N}} \psi_{\mathrm{I}}(\boldsymbol{x}) \begin{bmatrix} \boldsymbol{d}_{\mathrm{pI}} \\ \boldsymbol{d}_{\mathrm{wI}} \end{bmatrix}, \tag{20}$$

where $\psi_{\mathrm{I}}(\boldsymbol{x})$ is the shape function associated with node $\boldsymbol{x}_{\mathrm{I}}$, N denotes the number of nodes, and the in-plane and transverse displacements are expressed as $\boldsymbol{d}_{\mathrm{pI}} = [u_{0\mathrm{I}}\ v_{0\mathrm{I}}]^{\mathrm{T}}$, and $\boldsymbol{d}_{\mathrm{wI}} = [w_{0\mathrm{I}}]$, respectively. The shape function is written as

$$\psi_{\mathrm{I}}(\boldsymbol{x}) = C(\boldsymbol{x};\boldsymbol{x}-\boldsymbol{x}_{\mathrm{I}})\Phi(\boldsymbol{x}-\boldsymbol{x}_{\mathrm{I}}), \tag{21}$$

where $\Phi(\boldsymbol{x}-\boldsymbol{x}_{\mathrm{I}})$ denotes the kernel function, and the coefficient function $C(\boldsymbol{x};\boldsymbol{x}-\boldsymbol{x}_{\mathrm{I}})$ is expressed as

$$C(\boldsymbol{x};\boldsymbol{x}-\boldsymbol{x}_{\mathrm{I}}) = \boldsymbol{H}^{\mathrm{T}}(\boldsymbol{x}-\boldsymbol{x}_{\mathrm{I}})\boldsymbol{K}(\boldsymbol{x}), \tag{22}$$

$$\boldsymbol{H}^{\mathrm{T}}(\boldsymbol{x}-\boldsymbol{x}_{\mathrm{I}}) = \left[1, x-x_{\mathrm{I}}, y-y_{\mathrm{I}}, \left(x-x_{\mathrm{I}}\right)\left(y-y_{\mathrm{I}}\right), \left(x-x_{\mathrm{I}}\right)^2, \left(y-y_{\mathrm{I}}\right)^2\right], \tag{23}$$

$$\boldsymbol{K}(\boldsymbol{x}) = \left[k_0(x,y), k_1(x,y), k_2(x,y), k_3(x,y), k_4(x,y), k_5(x,y)\right]^{\mathrm{T}}, \tag{24}$$

where $\boldsymbol{H}^{\mathrm{T}}(\boldsymbol{x}-\boldsymbol{x}_{\mathrm{I}})$ and $\boldsymbol{K}(\boldsymbol{x})$ denote the quadratic basis and undetermined coefficient vectors, respectively. Then, the shape function is expressed as

$$\psi(\boldsymbol{x};\boldsymbol{x}-\boldsymbol{x}_{\mathrm{I}}) = \boldsymbol{K}^{\mathrm{T}}(\boldsymbol{x})\boldsymbol{H}(\boldsymbol{x}-\boldsymbol{x}_{\mathrm{I}})\Phi(\boldsymbol{x}-\boldsymbol{x}_{\mathrm{I}}). \tag{25}$$

When the shape function satisfies the reproduction conditions

$$\sum_{\mathrm{I}=1}^{\mathrm{N}} \psi_{\mathrm{I}}(\boldsymbol{x})\left(\boldsymbol{x}-\boldsymbol{x}_{\mathrm{I}}\right)^i = \delta_{i0}, i = 0,1,2,3,\ldots,n, \tag{26}$$

and

$$\boldsymbol{K}(\boldsymbol{x}) = \boldsymbol{M}^{-1}(\boldsymbol{x})\boldsymbol{H}(\boldsymbol{0}), \tag{27}$$

where

$$\boldsymbol{M}(\boldsymbol{x}) = \sum_{\mathrm{I}=1}^{\mathrm{N}} \boldsymbol{H}\left(\boldsymbol{x}-\boldsymbol{x}_{\mathrm{I}}\right)\boldsymbol{H}^{\mathrm{T}}\left(\boldsymbol{x}-\boldsymbol{x}_{\mathrm{I}}\right)\Phi\left(\boldsymbol{x}-\boldsymbol{x}_{\mathrm{I}}\right), \tag{28}$$

$$\boldsymbol{H}(\boldsymbol{0}) = [1,0,0,0,\cdots,0]^{\mathrm{T}}, \tag{29}$$

the shape function is expressed as

$$\psi_{\mathrm{I}}(\boldsymbol{x}) = \boldsymbol{H}^{\mathrm{T}}(\boldsymbol{0})\boldsymbol{M}^{-1}(\boldsymbol{x})\boldsymbol{H}\left(\boldsymbol{x}-\boldsymbol{x}_{\mathrm{I}}\right)\Phi\left(\boldsymbol{x}-\boldsymbol{x}_{\mathrm{I}}\right). \tag{30}$$

In the application of meshless method, the commonly used weight functions are cubic spline weight function, quartic spline weight function, exponential weight function, Gaussian weight function, etc. The choice of weight function depends on the problem, and the cubic spline function is generally adopted for the mechanical behavior of composite plates [13, 28–30, 33], which is given by

$$\Phi(r)=\begin{cases}\frac{2}{3}-4r^2+4r^3, & 0\le r<\frac{1}{2}\\ \frac{4}{3}-4r+4r^2-\frac{4}{3}r^3, & \frac{1}{2}\le r\le 1\\ 0, & r>1\end{cases} \tag{31}$$

where $r=\|\boldsymbol{x}-\boldsymbol{x}_{\mathrm{I}}\|/a_{\mathrm{I}}$, and a_{I} represents the radii of influence domain corresponding to the particle $\boldsymbol{x}_{\mathrm{I}}$, which should be appropriate to involve sufficient particles to ensure the invertible matrix and avoid the ill-conditioned system. Therefore, a_{I} is defined as $d_{\max}c_{\mathrm{I}}$, in which $d_{\max}$ denotes the scaling parameter ranging from 2 to 4, and c_{I} denotes the longest distance between the particle $\boldsymbol{x}_{\mathrm{I}}$ and neighbor points.

By substituting Eq. (20) into Eq. (19), the matrix form of discretized equations of composite plate is

$$\begin{bmatrix}\boldsymbol{M}_{\mathrm{p}} & \boldsymbol{0}\\ \boldsymbol{0} & \boldsymbol{M}_{\mathrm{w}}\end{bmatrix}\begin{bmatrix}\ddot{\boldsymbol{d}}_{\mathrm{p}}\\ \ddot{\boldsymbol{d}}_{\mathrm{w}}\end{bmatrix}+\left(\begin{bmatrix}\boldsymbol{K}_{\mathrm{p}} & \boldsymbol{0}\\ \boldsymbol{0} & \boldsymbol{K}_{\mathrm{w}}\end{bmatrix}+\begin{bmatrix}\boldsymbol{0} & \boldsymbol{K}_2\\ \boldsymbol{0} & \boldsymbol{0}\end{bmatrix}+\begin{bmatrix}\boldsymbol{0} & \boldsymbol{0}\\ \boldsymbol{K}_3 & \boldsymbol{0}\end{bmatrix}+\begin{bmatrix}\boldsymbol{0} & \boldsymbol{0}\\ \boldsymbol{0} & \boldsymbol{K}_4\end{bmatrix}\right)\begin{bmatrix}\boldsymbol{d}_{\mathrm{p}}\\ \boldsymbol{d}_{\mathrm{w}}\end{bmatrix}=\boldsymbol{0}, \tag{32}$$

where

$$\left[\boldsymbol{M}_{\mathrm{p}}\right]_{\mathrm{IJ}}=\int_{\Omega}\boldsymbol{B}_{\mathrm{pI}}^{\mathrm{T}}I_0\boldsymbol{B}_{\mathrm{pJ}}\mathrm{d}\Omega, \tag{33}$$

$$\left[\boldsymbol{M}_{\mathrm{w}}\right]_{\mathrm{IJ}}=\int_{\Omega}\psi_{\mathrm{I}}I_0\psi_{\mathrm{J}}\mathrm{d}\Omega, \tag{34}$$

$$\left[\boldsymbol{K}_{\mathrm{p}}\right]_{\mathrm{IJ}}=\int_{\Omega}\boldsymbol{B}_{\mathrm{lI}}^{\mathrm{T}}\boldsymbol{A}\boldsymbol{B}_{\mathrm{lJ}}\mathrm{d}\Omega, \tag{35}$$

$$\left[\boldsymbol{K}_{\mathrm{w}}\right]_{\mathrm{IJ}}=\int_{\Omega}\boldsymbol{B}_{\mathrm{bI}}^{\mathrm{T}}\boldsymbol{D}\boldsymbol{B}_{\mathrm{bJ}}\mathrm{d}\Omega, \tag{36}$$

$$\left[\boldsymbol{K}_2\right]_{\mathrm{IJ}}=\frac{1}{2}\int_{\Omega}\boldsymbol{B}_{\mathrm{lI}}^{\mathrm{T}}\boldsymbol{A}\boldsymbol{B}_{\mathrm{nJ}}\mathrm{d}\Omega, \tag{37}$$

$$\left[\boldsymbol{K}_3\right]_{\mathrm{IJ}}=\frac{1}{2}\int_{\Omega}\boldsymbol{B}_{\mathrm{nI}}^{\mathrm{T}}\boldsymbol{A}\boldsymbol{B}_{\mathrm{lJ}}\mathrm{d}\Omega, \tag{38}$$

$$\left[\boldsymbol{K}_4\right]_{\mathrm{IJ}}=\frac{1}{4}\int_{\Omega}\boldsymbol{B}_{\mathrm{nI}}^{\mathrm{T}}\boldsymbol{A}\boldsymbol{B}_{\mathrm{nJ}}\mathrm{d}\Omega, \tag{39}$$

$$\begin{aligned}&\boldsymbol{B}_{\mathrm{pI}}=\begin{bmatrix}\psi_{\mathrm{I}} & 0\\ 0 & \psi_{\mathrm{I}}\end{bmatrix},\boldsymbol{B}_{\mathrm{lI}}=\begin{bmatrix}\psi_{\mathrm{I},x} & 0\\ 0 & \psi_{\mathrm{I},y}\\ \psi_{\mathrm{I},y} & \psi_{\mathrm{I},x}\end{bmatrix},\\ &\boldsymbol{B}_{\mathrm{bI}}=\begin{bmatrix}-\psi_{\mathrm{I},xx}\\ -\psi_{\mathrm{I},yy}\\ -2\psi_{\mathrm{I},xy}\end{bmatrix},\boldsymbol{B}_{\mathrm{nI}}=\begin{bmatrix}w_{0,x} & 0\\ 0 & w_{0,y}\\ w_{0,y} & w_{0,x}\end{bmatrix}\begin{bmatrix}\psi_{\mathrm{I},x}\\ \psi_{\mathrm{I},y}\end{bmatrix}.\end{aligned} \tag{40}$$

Furthermore, Eq. (32) is divided into two parts as

$$\boldsymbol{M}_{\mathrm{p}}\ddot{\boldsymbol{d}}_{\mathrm{p}}+\boldsymbol{K}_{\mathrm{p}}\boldsymbol{d}_{\mathrm{p}}+\boldsymbol{K}_2\boldsymbol{d}_{\mathrm{w}}=\boldsymbol{0}, \tag{41}$$

$$\boldsymbol{M}_{\mathrm{w}}\ddot{\boldsymbol{d}}_{\mathrm{w}}+\boldsymbol{K}_3\boldsymbol{d}_{\mathrm{p}}+(\boldsymbol{K}_{\mathrm{w}}+\boldsymbol{K}_4)\boldsymbol{d}_{\mathrm{w}}=\boldsymbol{0}. \tag{42}$$

By substituting Eq. (41) into Eq. (42), we get

$$\boldsymbol{M}_{\mathrm{w}}\ddot{\boldsymbol{d}}_{\mathrm{w}}+(\boldsymbol{K}_{\mathrm{w}}+\boldsymbol{K}_4-\boldsymbol{K}_3\boldsymbol{K}_{\mathrm{p}}^{-1}\boldsymbol{K}_2)\boldsymbol{d}_{\mathrm{w}}=\boldsymbol{0}. \tag{43}$$

The transverse displacement is assumed as

$$\boldsymbol{d}_{\mathrm{wI}}=\psi_{\mathrm{I}}\bar{\boldsymbol{d}}_{\mathrm{wI}}\sin\omega t. \tag{44}$$

By substituting Eq. (44) into Eq. (43), the equations of motion are expressed as

$$\left[-\omega^2\boldsymbol{M}_{\mathrm{w}}\sin\omega t+\boldsymbol{K}_{\mathrm{w}}\sin\omega t+(\boldsymbol{K}_4-\boldsymbol{K}_3\boldsymbol{K}_{\mathrm{p}}^{-1}\boldsymbol{K}_2)(\sin\omega t)^3\right]\bar{\boldsymbol{d}}_{\mathrm{w}}=\boldsymbol{0}. \tag{45}$$

The weighted residual is taken along the time path [0, T/4] to consider the complete displacement path [0, $\bar{\boldsymbol{d}}_{\mathrm{wmax}}$], and the above equation is written as

Table 1 The material properties of PMMA matrix and CNT reinforcement

Matrix				Reinforcement			
E_{m} (GPa)	G_{m} (GPa)	ν_{m}	ρ_{m}(g/cm^3)	E_{CNT}^{11} (GPa)	E_{CNT}^{22} (GPa)	G_{CNT}^{12} (GPa)	ν_{CNT}^{12}
2.85	1.04	0.32	1.18	2349.7	213.93	701.22	0.188

Table 2 The efficiency parameters of elastic moduli for composite with different CNT volume fraction reinforcement

V_{CNT}	1%	2%	3%	4%	5%	6%	7%	8%	9%
η_1	0.819	0.802	0.785	0.770	0.753	0.739	0.725	0.712	0.700
η_2	1.062	1.291	1.498	1.682	1.842	1.980	2.094	2.186	2.254
η_3	1.476	1.541	1.648	1.796	1.987	2.219	2.494	2.810	3.168

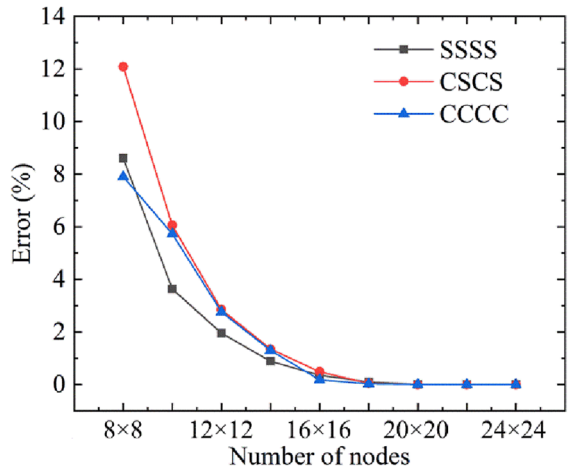

Fig. 2 Convergence curves of nonlinear frequency ratio for different node numbers with three boundary conditions

Table 3 Comparison of the nonlinear to linear frequency ratios for CNTRC plates ($a/b=1$, $b/h=100$, $V_{CNT}=0.17$)

Grading	W_{max}/h				
	0.2	0.4	0.6	0.8	1.0
UD					
Ref. [34]	1.0106	1.0420	1.0932	1.1692	1.2472
Ref. [35]	1.0322	1.1232	1.2603	1.4304	1.6231
Present	1.0207	1.1094	1.2870	1.5214	1.7849
FG-V					
Ref. [34]	1.0787	1.1714	1.2768	1.3900	1.5117
Ref. [35]	1.0454	1.1711	1.3549	1.5766	1.8244
Present	1.0279	1.1368	1.3340	1.5845	1.8630

$$\int_0^{T/4}\left[-\omega^2\boldsymbol{M}_{\mathrm{w}}\sin\omega t+\boldsymbol{K}_{\mathrm{w}}\sin\omega t+(\boldsymbol{K}_4-\boldsymbol{K}_3\boldsymbol{K}_{\mathrm{p}}^{-1}\boldsymbol{K}_2)(\sin\omega t)^3\right]\bar{\boldsymbol{d}}_{\mathrm{w}}\sin\omega t\mathrm{d}t=\boldsymbol{0}. \tag{46}$$

The discretized nonlinear vibration equation without the time term is expressed as

$$\left[\boldsymbol{K}_{\mathrm{w}}+\frac{3}{4}(\boldsymbol{K}_4-\boldsymbol{K}_3\boldsymbol{K}_{\mathrm{p}}^{-1}\boldsymbol{K}_2)-\omega^2\boldsymbol{M}_{\mathrm{w}}\right]\bar{\boldsymbol{d}}_{\mathrm{w}}=\boldsymbol{0}. \tag{47}$$

The linearized updated mode (LUM) method is adopted to solve the nonlinear vibration equation of the composite plates. The following linear equations are solved to obtain linear eigenvalue and eigenvector via

$$\left(-\omega^2\boldsymbol{M}_{\mathrm{w}}+\boldsymbol{K}_{\mathrm{w}}\right)\bar{\boldsymbol{d}}_{\mathrm{w}}=\boldsymbol{0}. \tag{48}$$

The linear eigenvalue λ_{L} and eigenvector ω_{L} are normalized to obtain the initial input data by the assumed amplitude αh as

$$\omega_{\mathrm{i}}=\frac{\alpha h}{(\omega_{\mathrm{L}})_{\max}}\omega_{\mathrm{L}}, \tag{49}$$

where $(\omega_{\mathrm{L}})_{\max}$ denotes the amplitude of linear eigenvector, and α is the amplitude parameter. The normalized eigenvector is substituted into the following equation to solve the nonlinear stiffness matrix as

$$\boldsymbol{K}_{\mathrm{NL}}=\boldsymbol{K}_{\mathrm{w}}+\frac{3}{4}\left(\boldsymbol{K}_4-\boldsymbol{K}_3\boldsymbol{K}_{\mathrm{p}}^{-1}\boldsymbol{K}_2\right) \tag{50}$$

$$\left(-\omega^2\boldsymbol{M}_{\mathrm{w}}+\boldsymbol{K}_{\mathrm{NL}}\right)\bar{\boldsymbol{d}}_{\mathrm{w}}=\boldsymbol{0}. \tag{51}$$

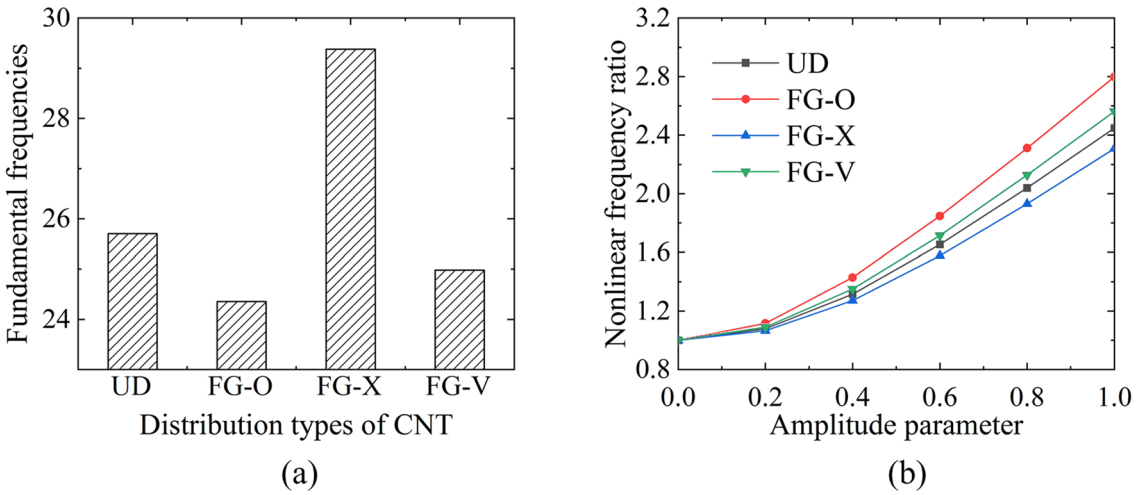

Fig. 3 Comparison of **a** fundamental frequencies and **b** nonlinear frequency ratios of UD, FG-O, FG-X, and FG-V of square composite plate ($a/b=1$, $b/h=10$, $V_{CNT}=2\%$)

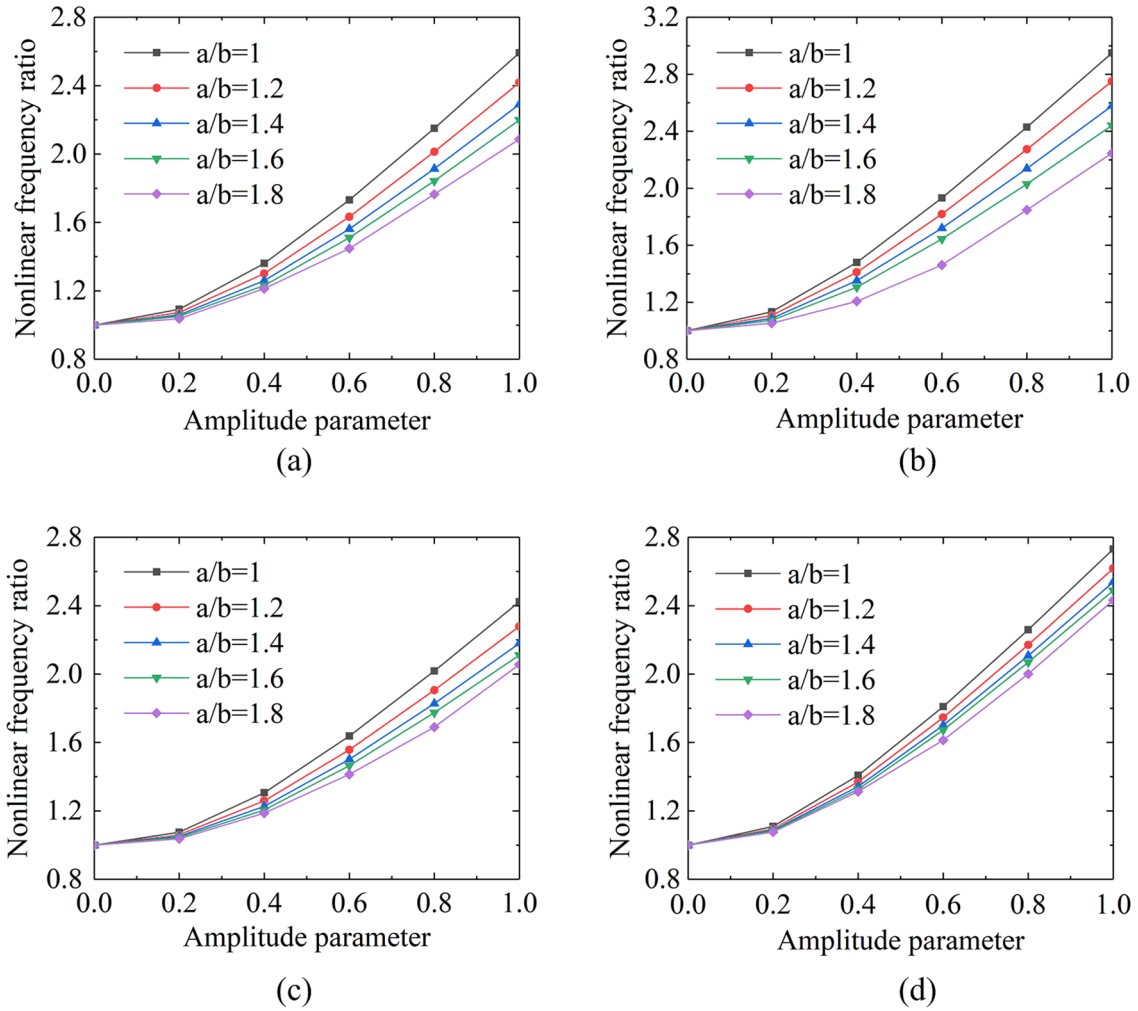

Fig. 4 Nonlinear frequency ratio–amplitude curve of FG-CNTRC plates including **a** UD; **b** FG-O; **c** FG-X; **d** FG-V with different aspect ratios ($b/h = 10$, $V_{CNT} = 4\%$)

Afterwards, Eq. (51) is solved to regenerate the eigenvalue λ_i and eigenvector ω_i, where i denotes the i-th iteration.

The amplitude αh in Eq. (49) is used to normalize the new eigenvalue λ_i and eigenvector ω_i

$$\omega_i = \frac{\alpha h}{(\omega_i)_{\max}} \omega_i. \tag{52}$$

Then, the nonlinear stiffness matrix is calculated, and the new eigenvalues λ_{i+1} and eigenvectors ω_{i+1} are generated.

Finally, the convergence is checked by

$$\left| \frac{\lambda_{i+1} - \lambda_i}{\lambda_{i+1}} \right| < C_r, \tag{53}$$

where C_r ranges between 10^{-4} and 10^{-6}. If the condition is satisfied, the nonlinear frequency ratios versus amplitude parameter are recorded, otherwise, it is returned to Eq. (52).

Results and Discussion

In this section, the nonlinear free vibration of CNTRC plate is analyzed. The material parameters of FG-CNTRC plates are quoted from the MD simulation of our previous study [19]. The Poly (methyl methacrylate), referred to as PMMA, is considered as the matrix. Long CNT is used as reinforcement throughout the polymer matrix along the axial direction, and the material parameters of matrix and CNT reinforcement are listed in Table 1. The considered CNT volume fraction and corresponding efficiency parameters of (5, 5) SWCNT are shown in Table 2. Different boundary conditions are considered, where "S" represents simply supported, and "C" represents clamped boundary conditions. Three combined boundary conditions are adopted including four edges simply supported (SSSS), a pair of opposite edges clamped and left edges simply supported (CSCS), and four

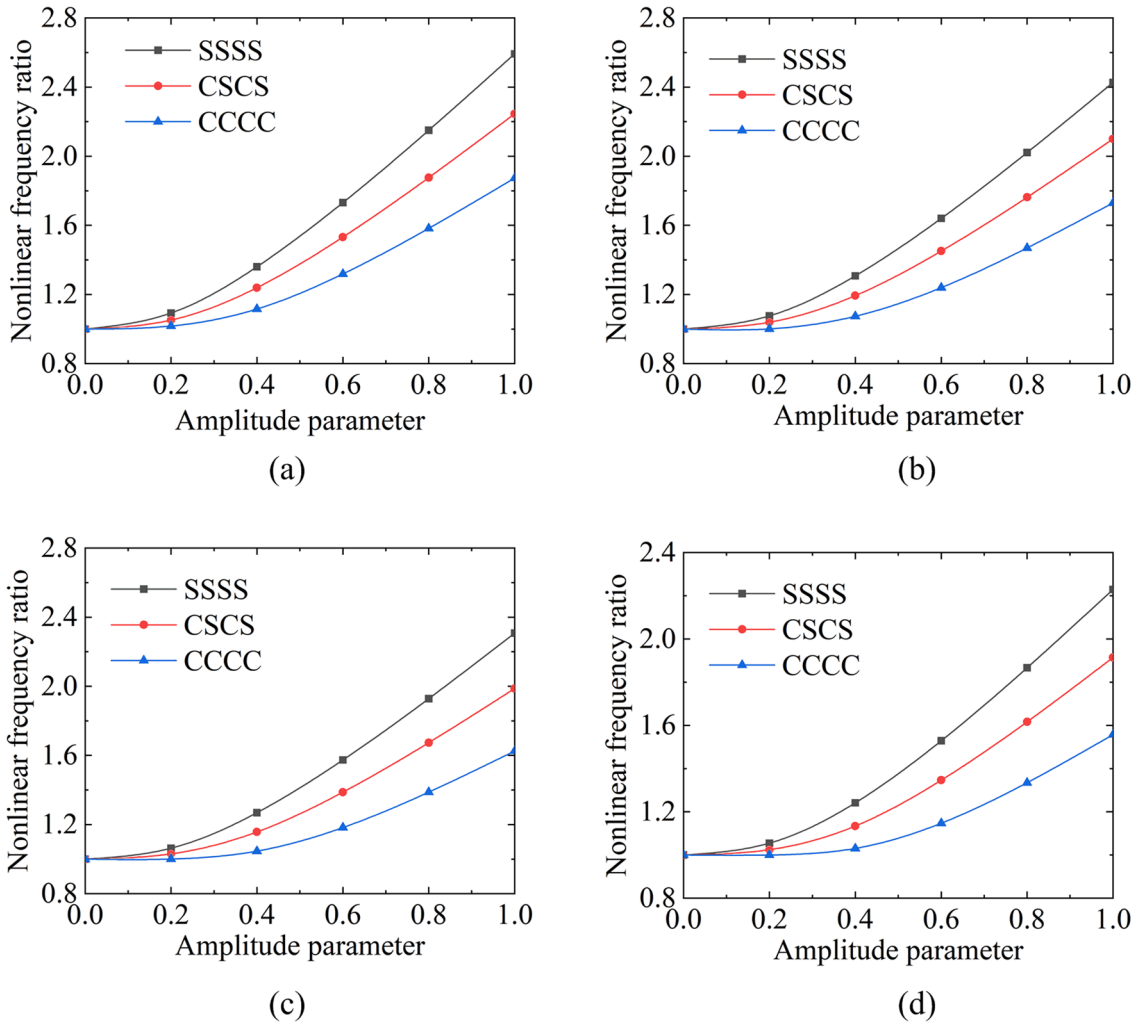

Fig. 5 Nonlinear frequency ratio–amplitude curve of square UD CNTRC plates under different boundary conditions with CNT volume fraction **a** $V_{CNT}=2\%$; **b** $V_{CNT}=4\%$; **c** $V_{CNT}=6\%$; **d** $V_{CNT}=8\%$ ($a/b=1$, $b/h=10$)

edges fully clamped (CCCC). Unless otherwise mentioned, the plate is considered with all edges simply supported.

For convenience, the linear and nonlinear frequencies of FG-CNTRC plates are nondimensionalized using the formula $\overline{\omega}=\omega\left(a^2/h\right)\sqrt{\rho_m/E_m}$. The nonlinear frequency ratio is defined as ω_{NL}/ω_L, where ω_L and ω_{NL} represent the linear and nonlinear frequencies, respectively. The nondimensional maximum amplitude of the composite plate is W_{max}/h, which is also called as amplitude parameter. The CNTRC plates are considered with four distributions, namely UD, FG-O, FG-X and FG-V, and the thickness is taken as $h=0.001$ m.

Convergence and Validation Study

The convergence study is carried out, and the errors of the nonlinear frequency ratios with different node numbers for the UD CNTRC plates are illustrated under three boundary conditions (SSSS, CSCS and CCCC) with W_{max}/h=0.2 in Fig. 2. The aspect ratio a/b is 1, width to thickness ratio a/h is 10, and CNT volume ratio is $V_{CNT}=2\%$. It is observed that the error decreases as the node number increases for all boundary conditions. When the number of nodes increases from 18×18 to 24×24, the error remains stable around 0, and hence, the mesh consists of 18×18 nodes is adopted in the following studies.

The nonlinear frequency ratios of square simply supported plates are compared with FEM in Table 3. The nonlinear frequency ratios of UD and FG-V CNTRC plates are depicted, and the amplitude ratios are set as $W_{max}/h=0.2$, 0.4, 0.6, 0.8 and 1.0, respectively. The present results are in

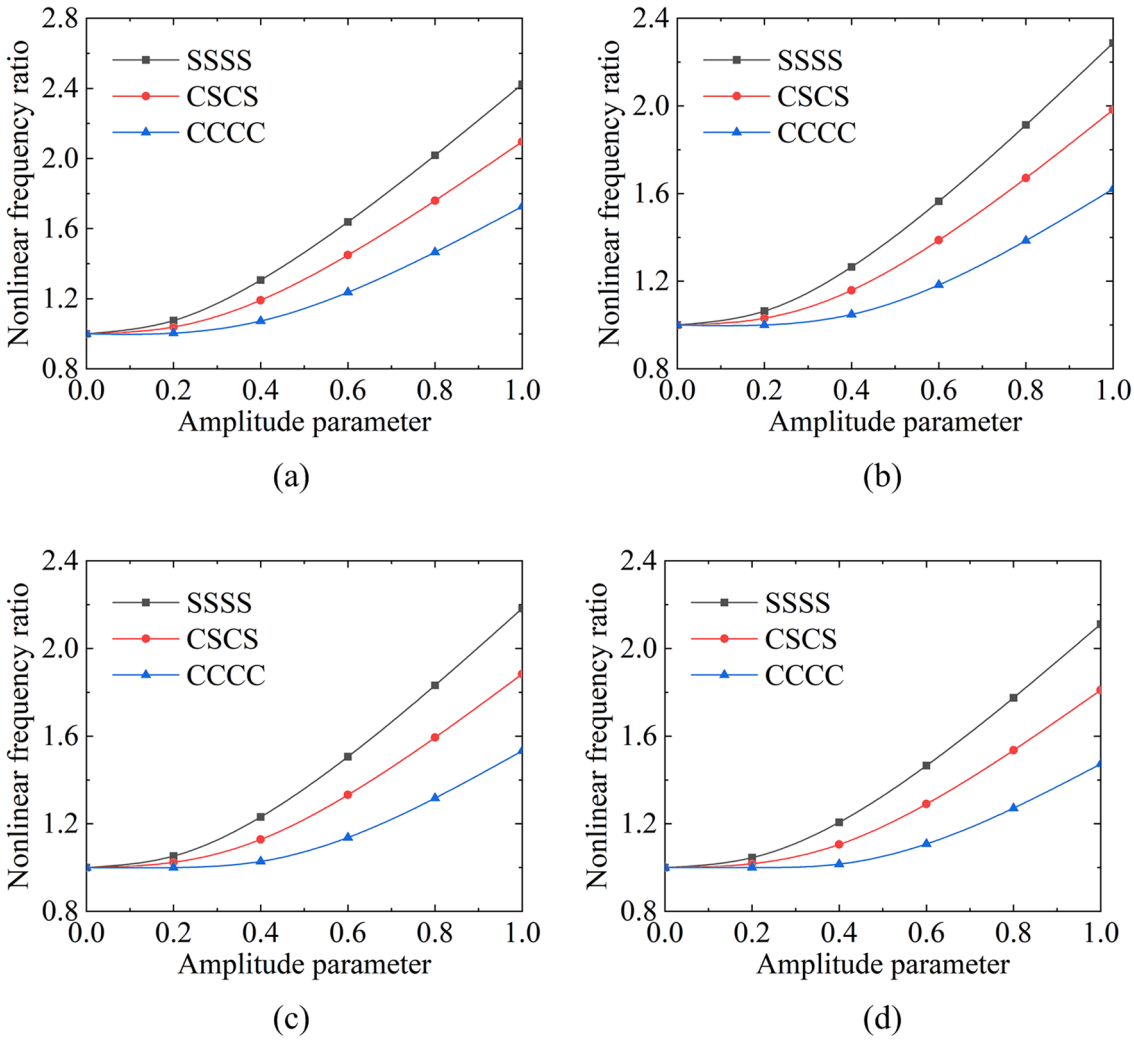

Fig. 6 Nonlinear frequency ratio–amplitude curve of square FG-X CNTRC plates under different boundary conditions with CNT volume fraction **a** $V_{CNT}=2\%$; **b** $V_{CNT}=4\%$; **c** $V_{CNT}=6\%$; **d** $V_{CNT}=8\%$ ($a/b=1$, $b/h=10$)

good agreements with Refs. [34] and [35], which demonstrate that the nonlinear frequency ratio increases with the increase of amplitude parameter.

Parametric Studies

The influence of CNT distribution on the fundamental frequency is shown in Fig. 3a, which indicates that among the four CNT distributions of CNTRC plates including UD, FG-X, FG-O and FG-V, FG-X has the highest frequency, and FG-O CNTRC plates have the lowest one. The composite plate with the reinforcement distributions close to the top and bottom surfaces are more efficient in increasing the stiffness of CNTRC plate than those distributions near the mid-plane. Meanwhile, the nonlinear frequency ratios of the composite plate are displayed in Fig. 3b. With the increase of amplitude parameter, the nonlinear frequency ratio increases obviously. When the composite plate has a high dimensionless fundamental frequency, the corresponding nonlinear frequency ratio is low relatively. The nonlinear frequency ratio of the composite plates decreases with the increase of the stiffness, because of the transverse deformation of the composite plate and that the influence of geometrical nonlinearity decrease with the increase of stiffness. Figure 4 presents the influence of aspect ratio ($a/b=1.0$, 1.2, 1.4, 1.6 and 1.8) on the nonlinear frequency ratio of four FG-CNTRC square plates, which reveals that the nonlinear frequency ratio of CNTRC plates decreases gradually with the increase of aspect ratio.

The influence of boundary condition on the nonlinear frequency ratio of UD and FG-X CNTRC plates with different CNT volume fractions are shown in Figs. 5 and 6, respectively. The nonlinear frequency ratios of CNTRC plates with SSSS boundary condition are generally higher than those

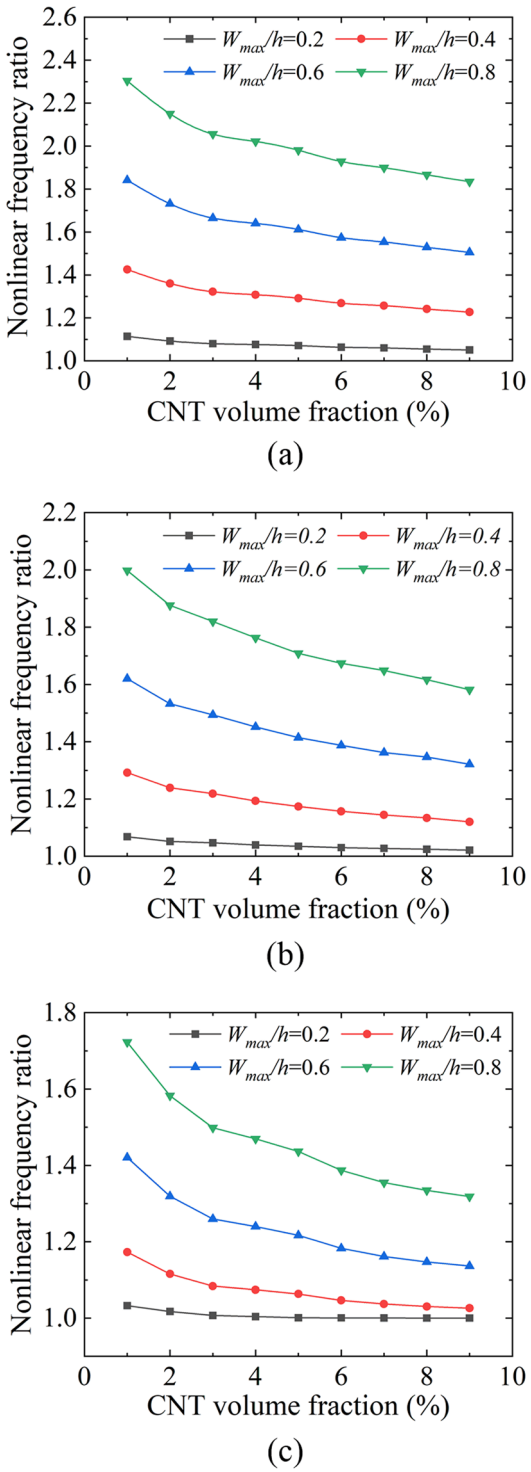

Fig. 7 Nonlinear frequency ratio of square CNTRC plates with different amplitude parameters under the boundary condition **a** SSSS; **b** CSCS; **c** CCCC ($a/b = 1$, $b/h = 10$)

with CSCS boundary condition, and the nonlinear frequency ratios with CCCC boundary condition are usually lower than those with CSCS boundary condition. The similar nonlinear vibration behaviors of FG-O and FG-V CNTRC plates are consistent with UD and FG-X CNTRC plates for the above three boundary conditions.

Figures 7 and 8 depict the effects of reinforcement content and amplitude parameter on the nonlinear vibration of the FG-CNTRC plates, respectively, in which the variation range of CNT volume fractions are 1%, 2%, 3%,4%, 5%, 6%, 7%, 8% and 9%, and the scope of amplitude parameters are from 0.2 to 1. The effect of the amplitude parameter on nonlinear frequency ratio of square CNTRC plates is demonstrated in Fig. 7, which indicate that the nonlinear frequency ratio increases with the amplitude parameter increases, furthermore, the downward trend of curve declines apparently with the increase of amplitude parameters. Figure 8 illustrates that as the CNT volume fraction increases from 1 to 9% and the amplitude parameter is taken as 1, the stiffness of the plate increases correspondingly resulting in the decrease of the nonlinear frequency ratio. For the four distribution patterns, the decline amplitude of nonlinear frequency ratio curve almost decreases gradually, which demonstrates that the reinforcement effect of CNT on the stiffness of composite plate is not linearly related to the CNT volume fraction.

Conclusions

The nonlinear vibration behavior for CNTRC plate is presented, and a parametric study of CNTRC plates with different boundary conditions, aspect ratios, CNT volume fractions and distributions is carried out in detail. The comparison analysis proves that the nonlinear frequency ratio of FG-CNTRC plates obtained by RKPM is consistent with FEM. Numerical results reveal that the nonlinear frequency ratio is increased by increasing the amplitude parameter. Among the four distributions, FG-X CNTRC plates have the highest frequency, and FG-O CNTRC plates have the lowest. On the contrary, FG-X CNTRC plates have the lowest nonlinear frequency ratio, and FG-O CNTRC plates have the highest. Hence, the composite plate with the reinforcement close to the top and bottom surfaces are more efficient in increasing the stiffness of CNTRC plates than those near the mid-plane. The nonlinear frequency ratio is reduced by increasing the CNT volume fraction. As the aspect ratio increases, the nonlinear frequency ratio decreases slowly. The present results indicate that the nonlinear frequency

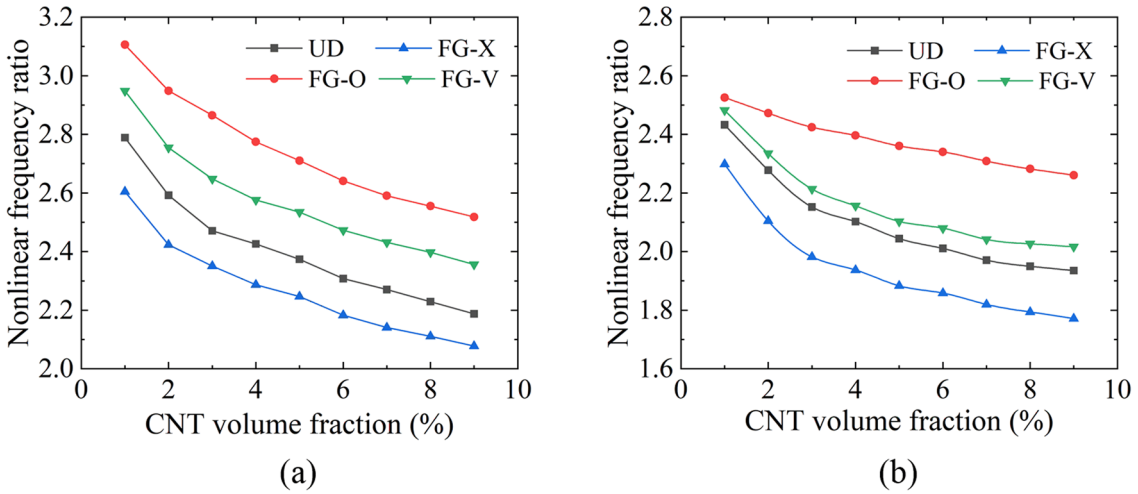

Fig. 8 Nonlinear frequency ratio of CNTRC plates with the increase of CNT volume fraction with the aspect ratio **a** $a/b=1$; **b** $a/b=1.5$

ratio decreases with the increase of boundary constraint of the FG-CNTRC plates.

Acknowledgements The authors gratefully acknowledge the support of National Natural Science Foundation of China through Grant No. 12072003, 11702006 and 11832002.

Declarations

Conflict of Interest The authors declare that there is no conflict of interest regarding the publication of this paper.

References

1. Treacy MMJ, Ebbesen TW, Gibson JM (1996) Exceptionally high Young modulus observed for individual carbon nanotubes. Nature 381:678–680
2. Philippe P, Wang ZL, Daniel U, de Heer WA (1999) Electrostatic deflections and electromechanical resonances of carbon nanotubes. Science 283:1513–1515
3. Salvetat JP, Briggs GAD, Bonard JM, Bacsa RR, Kulik AJ, Stöckli T et al (1999) Elastic and shear moduli of single-walled carbon nanotube ropes. Phys Rev Lett 82:944–947
4. Coleman JN, Khan U, Blau WJ, Gunko YK (2006) Small but strong: a review of the mechanical properties of carbon nanotube-polymer composites. Carbon N Y 44:1624–1652
5. Qian D, Dickey EC, Andrews R, Rantell T (2000) Load transfer and deformation mechanisms in carbon nanotube-polystyrene composites. Appl Phys Lett 76:2868–2870
6. Kilbride BE, Coleman JN, Fraysse J, Fournet P, Cadek M, Drury A et al (2002) Experimental observation of scaling laws for alternating current and direct current conductivity in polymer-carbon nanotube composite thin films. J Appl Phys 92:4024–4030
7. Biercuk MJ, Llaguno MC, Radosavljevic M, Hyun JK, Johnson AT, Fischer JE (2002) Carbon nanotube composites for thermal management. Appl Phys Lett 80:2767–2769
8. Bever MB, Duwez PE (1972) Gradients in composite materials. Mater Sci Eng 10:1–8
9. Ning Z, Tahir K, Haomin G, Shaoshuai S, Wei ZWZ (2019) Functionally graded materials: an overview of stability, buckling, and free vibration analysis. Adv Mater Sci Eng 2019:1–18
10. Naebe M, Shirvanimoghaddam K (2016) Functionally graded materials a review of fabrication and properties. Appl Mater Today 5:223–245
11. Shen HS (2009) Nonlinear bending of functionally graded carbon nanotube-reinforced composite plates in thermal environments. Compos Struct 91:9–19
12. Yu Y, Shen HS (2020) A comparison of nonlinear vibration and bending of hybrid CNTRC/metal laminated plates with positive and negative Poisson's ratios. Int J Mech Sci 183:105790
13. Wang JF, Yang JP, Tam LH, Zhang W (2021) Molecular dynamics-based multiscale nonlinear vibrations of PMMA/CNT composite plates. Mech Syst Signal Process 153:107530
14. Wang JF, Cao SH, Zhang W (2021) Thermal vibration and buckling analysis of functionally graded carbon nanotube reinforced composite quadrilateral plate. Eur J Mech A/Solids 85:104105
15. Chiker Y, Bachene M, Guemana M, Attaf B, Rechak S (2020) Free vibration analysis of multilayer functionally graded polymer nanocomposite plates reinforced with nonlinearly distributed carbon-based nanofillers using a layer-wise formulation model. Aerosp Sci Technol 104:105913
16. Tang H, Dai HL (2021) Nonlinear vibration behavior of CNTRC plate with different distribution of CNTs under hygrothermal effects. Aerosp Sci Technol 115:106767
17. Shen HS, Zhang CL (2010) Thermal buckling and postbuckling behavior of functionally graded carbon nanotube-reinforced composite plates. Mater Des 31:3403–3411
18. Han Y, Elliott J (2007) Molecular dynamics simulations of the elastic properties of polymer/carbon nanotube composites. Comput Mater Sci 39:315–323

19. Wang JF, Yang JP, Tam LH, Zhang W (2022) Effect of CNT volume fractions on nonlinear vibrations of PMMA/CNT composite plates: a multiscale simulation. Thin-Walled Struct 170:108513
20. Mehar K, Panda SK, Mahapatra TR (2017) Theoretical and experimental investigation of vibration characteristic of carbon nanotube reinforced polymer composite structure. Int J Mech Sci 133:319–329
21. Mehar K, Panda SK (2018) Elastic bending and stress analysis of carbon nanotube-reinforced composite plate: experimental, numerical, and simulation. Adv Polym Technol 37:1643–1657
22. Fantuzzi N, Tornabene F, Bacciocchi M, Dimitri R (2017) Free vibration analysis of arbitrarily shaped functionally graded carbon nanotube-reinforced plates. Compos Part B 115:384–408
23. Ankit G, Talha M (2017) Large amplitude free flexural vibration analysis of finite element modelled FGM platesusing new hyperbolic shear and normal deformation theory. Aerosp Sci Technol 67:287–308
24. Peng YX, Zhang AM, Ming FR (2021) Particle regeneration technique for Smoothed Particle Hydrodynamics in simulation of compressible multiphase flows. Comput Methods Appl Mech Eng 376:113653
25. Luke E, Collins E, Blades E (2012) A fast mesh deformation method using explicit interpolation. J Comput Phys 231:586–601
26. Jun S, Liu WK, Belytschko T (1998) Explicit reproducing kernel particle methods for large deformation problems. Int J Numer Methods Eng 41:137–166
27. Wang JF, Zhang W (2018) An equivalent continuum meshless approach for material nonlinear analysis of CNT-reinforced composites. Compos Struct 188:116–125
28. Qin X, Shen Y, Chen W, Yang J, Peng LX (2021) Bending and free vibration analyses of circular stiffened plates using the FSDT mesh-free method. Int J Mech Sci 202–203:106498
29. Wang JF, Shi SQ, Yang JP, Zhang W (2021) Multiscale analysis on free vibration of functionally graded graphene reinforced PMMA composite plates. Appl Math Model 98:38–58
30. Fallah N, Delzendeh M (2018) Free vibration analysis of laminated composite plates using meshless finite volume method. Eng Anal Bound Elem 88:132–144
31. Esfahani SG, Sarrami-Foroushani S, Azhari M (2021) On the use of reproducing kernel particle finite strip method in the static, stability and free vibration analysis of FG plates with different boundary conditions and diverse internal supports. Appl Math Model 92:380–409
32. Shukla V, Vishwakarma PC, Singeh J, Singh J (2019) Vibration analysis of angle-ply laminated plates with RBF based meshless approach. Mater Today Proc 18:4605–4612
33. Wang JF, Yang JP, Lai SK, Zhang W (2020) Stochastic meshless method for nonlinear vibration analysis of composite plate reinforced with carbon fibers. Aerosp Sci Technol 105:105919
34. Kazemi M, Rad MHG, Hosseini SM (2021) Nonlinear dynamic analysis of FG carbon nanotube/epoxy nanocomposite cylinder with large strains assuming particle/matrix interphase using MLPG method. Eng Anal Bound Elem 132:126–145
35. Liu WK, Jun S, Zhang YF (1995) Reproducing kernel particle methods. Int J Numer Methods Fluids 20:1081–1106